JSR

Journal of Sedimentary Research, 2024, v. 94, 302–312
Research Article
DOI: 10.2110/jsr.2023.118

SCOUR-DEPTH VARIABILITY CONTROLS CHANNEL-SCALE STRATIGRAPHY IN EXPERIMENTAL BRAIDED RIVERS

FEIFEI ZHAO,[1] VAMSI GANTI,[1,2] AND AJAY B. LIMAYE[3]
[1]*Department of Geography, University of California Santa Barbara, Santa Barbara, California 93117, U.S.A.*
[2]*Department of Earth Science, University of California Santa Barbara, Santa Barbara, California 93106, U.S.A.*
[3]*Department of Environmental Sciences, University of Virginia, Charlottesville, Virginia 22903, U.S.A.*
e-mail: xiafeizhao@ucsb.edu

ABSTRACT: **Braided rivers distribute sediment across landscapes, often forming wide channel belts that are preserved in stratigraphy as coarse-grained deposits. Theoretical work has established quantitative links between the depth distribution of formative channels in a braided river and the geometry of their preserved strata. However, testing these predictive relationships between geomorphic process and stratigraphic product requires examining how braided rivers and their deposits coevolve, with high resolution in both space and time. Here, using a series of four runs of a physical experiment, we examine the controls of water discharge and slope on the resulting geometry of preserved deposits. Specifically, we focus on how a twofold variation in water discharge and initial riverbed slope affects the spatiotemporal distribution of channel depths and the geometry of preserved deposits of a braided river. We find that the channel depths in the laboratory experiment are described by a two-parameter gamma distribution and the deepest scours correspond to zones of erosion at channel-belt margins and channel-thread confluences in the channel belt. We use a reduced-complexity flow model to reconstruct flow depths, which were shallower compared to channel thalweg depths. Synthetic stratigraphy built from timeseries of topographic surfaces shows that the distribution of cut-and-fill-unit thickness is invariant across the experiments and is determined by the variability in scour depths. We show that the distribution of cut-and-fill-unit thickness can be used to reconstruct formative-channel-depth distributions and that the mean thickness of these units is 0.31 to 0.62 times the mean formative flow depth across all experiments. Our results suggest that variations in discharge and slope do not translate to measurable differences in preserved cut-and-fill-unit thickness, suggesting that changes in external forcings are likely to be preserved in braided river deposits only when they exceed a certain threshold of change.**

INTRODUCTION

Braided rivers form varied deposits, including sand or gravel bars, which are often partly or sometimes completely preserved in the fluvial rock record. Quantifying patterns in these deposits is essential for reconstructing ancient morphodynamics and fluvial sediment supply (Paola and Mohrig 1996; Bridge and Tye 2000; Mohrig et al. 2000; Hajek and Edmonds 2014; Holbrook and Wanas 2014), and for characterizing subsurface deposits to aid hydrocarbon exploration and aquifer characterization (e.g., Martin 1993; Anderson et al. 1999). Erosional surfaces define the architecture of fluvial stratigraphy, and major erosional surfaces are often thought to reflect variations in allogenic processes (i.e., sea level, climate, tectonics) (e.g., Miall 1985; Schlager 1993; Holbrook 2001). However, autogenic processes can also exert a primary control on the formation of erosional surfaces (e.g., Strong and Paola 2008; Trower et al. 2018; Ganti et al. 2019), particularly channel scours at anabranch confluences (Ashmore 1993, 2013; Willis and Behrensmeyer 1994; Best and Ashworth 1997; Bridge 2003; Ashmore and Gardner 2008). Confluence scours, which occur at the intersection of channel threads around major mid-channel bars in braided rivers, can be as deep as five times the mean channel depth (Best and Ashworth 1997; Sambrook Smith et al. 2005; Huber and Huggenberger 2015; Sambrook Smith et al. 2019) and provide the local accommodation for the sediments to be subsequently preserved (Paola and Borgman 1991; Sambrook Smith et al. 2019). The deposits bounded by successive erosional surfaces created by channel scours represent cycles of river aggradation and subsequent incision, or cut-and-fill cycles (Mohrig et al. 2000; Straub and Esposito 2013; Holbrook and Miall 2020), which are readily recognized in field outcrops. Understanding how channel depth varies under various allogenic conditions (e.g., water discharge) and how the distribution of scours relates to the geometry of cut-and-fill units is valuable for inferring paleoenvironmental conditions (Ashmore and Parker 1983; Best and Ashworth 1997; Miall and Jones 2003; Marren 2005; Sambrook Smith et al. 2006; Gardner and Ashmore 2011).

Existing theory establishes quantitative links between the distribution of local channel depths in braided rivers and the resulting stratigraphic architecture (Allen 1984; Paola and Borgman 1991; Bridge and Best 1997). In particular, Paola and Borgman (1991) posited that the variability of channel depths in a braided river can be described by a two-parameter Gamma distribution:

$$f(h_{channel}) = \frac{{h_{channel}}^{\alpha-1} e^{-h_{channel}/\beta}}{\beta^{\alpha}\Gamma(\alpha)} \quad (1)$$

where $\Gamma(\alpha)$ is the standard gamma function, $h_{channel}$ is the channel depth, e is Euler's number approximately equal to 2.718, β is the mean value of the

Published Online: June 2024
 1527-1404/24/094-302

exponential tail of the probability density for channel depth, and α is the shape parameter of the distribution. Paola and Borgman (1991) further derived a probability density function linking channel-depth distribution and preserved cut-and-fill-unit thickness (i.e., thickness of the deposit between successive erosional surfaces at the channel scale), herein referred to as "unit thickness," in a setting with no net sedimentation:

$$p(s) = \frac{\frac{1}{\beta}e^{-\frac{s}{\beta}}\left(e^{-\frac{s}{\beta}} + \frac{s}{\beta} - 1\right)}{\left(1 - e^{-\frac{s}{\beta}}\right)^2}; s > 0 \quad (2)$$

where $p(s)$ is the probability density for unit thickness s. Equation 2 predicts that the mean preserved unit thickness is related to the distribution of formative channel depths as

$$\overline{s} = 1.645\beta \quad (3)$$

This theoretical work linking surface processes and the preserved stratigraphy has been extensively tested at the bedform scale (e.g., Bridge and Best 1997; Leclair 2002; Jerolmack and Mohrig 2005; Ganti et al. 2013; Das et al. 2022). However, it is largely untested at the scale of bars in fluvial systems; an exception to this is a study by van de Lageweg et al. (2013a, 2013b), who analyzed the evolution of braided and meandering rivers in an experimental basin.

In spite of their development at small spatial and temporal scales, deposits formed in physical models enable quantifying deposit geometry under controlled conditions (Peakall et al. 2007; Paola et al. 2009; van de Lageweg et al. 2013a). For example, van de Lageweg et al. (2013b) used reduced-scale physical experiments to test the relationship between channel-scale morphology and unit thickness under constant and varied discharge conditions. Their findings align with the variability-dominated preservation model (cf. Reesink et al. 2015) proposed by Paola and Borgman (1991) and show that unit thickness was equivalent to 10 to 40% of the mean channel depth. However, the relationship between confluence scours and deposit geometry, and the independent effects of water discharge and bed slope on braided river architecture have yet to be tested.

We aimed to investigate how sensitive the preserved deposits of braided rivers are to differences in water discharge and bed slope. To this end, a recent set of physical experiments that captured the development of four braided rivers using time series topography measurements (Limaye 2020) enables systematic testing for the relationships between channel depths, scours, and preserved unit thickness. We compare the observations in the laboratory experiments to the Paola and Borgman (1991) theory, which predicts unit thickness as a function of channel-depth distribution (Equation 2). We also ran a two-dimensional flow model, CAESAR-lisflood, to reconstruct flow depths from digital elevation models (DEMs), which are difficult to obtain in the laboratory without disturbing sediment transport and with the same spatial resolution as topographic data (van Dijk et al. 2013).

METHODS

Experiment Setup and Data Collection

The experiments were performed and originally documented by Limaye (2020). The experiments were conducted in a basin 37 m long and 2.7 m wide at St. Anthony Falls Laboratory, University of Minnesota. The experiment consisted of four runs (Table 1), each with constant sediment and water discharge, in which the river evolved from a straight initial condition to a braided river that gradually developed a wider channel belt. Water discharge (Q) and initial bed slope (S) were varied independently, and each by a factor of two (Table 1), resulting in a fourfold variation in stream power across the experiments. We consider slope as an independent variable in our analysis because the time for significant slope change is much longer than the total duration of each run (Limaye 2020). However, we note that slope is not an independent variable in natural river systems but is instead set by the balance between water supply and sediment supply (Parker 1978; Dade and Friend 1998; Dunne and Jerolmack 2020; Paola 2000). For all runs, the initial channel depth was fixed at 3 cm, sediment was fed only to prevent scour at the inlet, and the median grain size of bed sediment (D_{50}) is 0.42 mm.

TABLE 1.—*Parameters for each run of the experiment. More details can be found in Limaye (2020).*

	Run 1	Run 2	Run 3	Run 4
Discharge, Q (L/s)	0.25	0.12	0.25	0.12
Sediment discharge, Q_s (L/s)	0.001	0.002	0.001	0.002
Initial channel-bed slope, S	0.01	0.01	0.02	0.02

To capture the morphodynamic evolution of the channel belt, detailed topographic measurements were made using an optical and laser-line scanner to generate DEMs with a grid spacing of 2 mm and submillimeter vertical precision. Bed-elevation data were collected at intervals from 1 to 5 hours by pausing the experiment and draining the surface water before each topography scan. Limaye (2020) mapped channel belts from these topography data by differencing successive DEMs and applying a change threshold of 3 mm to generate a mask of topography change that was refined using binary image operations. In each run the surface evolved at a different pace and developed landforms at varied scales but showed classic evolution from a straight channel to form alternate bars, meandering-channel threads, braided channels, and eventually wider channel belts (e.g., Friedkin 1945; Ashmore 1991). To systematically compare the evolution of the channel belt across all runs, Limaye (2020) recast run time in a dimensionless form as

$$t^* = \frac{tgD_{50}^2}{QS^{2/3}} \quad (4)$$

where t is the run time of the experiment and g is acceleration due to gravity. Using this non-dimensional formulation for time and a non-dimensional form of the channel-belt width, the growth trajectories of the four channel belts are nearly identical after accounting for differences in water discharge and bed slope. Limaye (2020) showed that three distinct phases occur at similar dimensionless times: 1) channel-belt widening associated with a single-thread channel planform ($t^* = 0$ to 2000), 2) logarithmic growth in channel-belt width, associated with a braided planform ($t^* = 2000$ to 10,000), 3) and channel-belt maturity, where topographic change declines due to a decline in shear stress caused by decreasing flow depth as the channel widens ($t^* > 10{,}000$) (Fig. 1).

Quantifying Channel Depths and the Geometry of Preserved Deposits

For each run, we quantified the channel depths and the preserved unit thickness using the time series of bed-elevation data. Analogous to thalweg depth measurements, we defined channel depth ($h_{channel}$) as the vertical elevation difference between the channel-belt topography and the average adjacent undisturbed topography outside of the channel-belt masks, as previously generated by Limaye (2020) (Fig. 2). We defined the largest channel depths (greater than the 75th percentile of channel-depth distribution) at each time step as the scour depths (Fig. 2). We also refer to deepest scours as $>$ 95th percentile channel depths at each time step. We computed $h_{channel}$ from every DEM throughout each run and examined the spatial distribution of the scours in the channel belt. We then compared the observed channel-depth distribution with a two-parameter gamma distribution and estimated the scale parameter from the best-fitting Gamma distribution (see Equation 1).

We constructed synthetic stratigraphic cross sections for every 2 mm using the bed-elevation time series, where we removed deposited sediment that was later eroded (e.g., Ganti et al. 2011; Straub et al. 2012). This sequence of

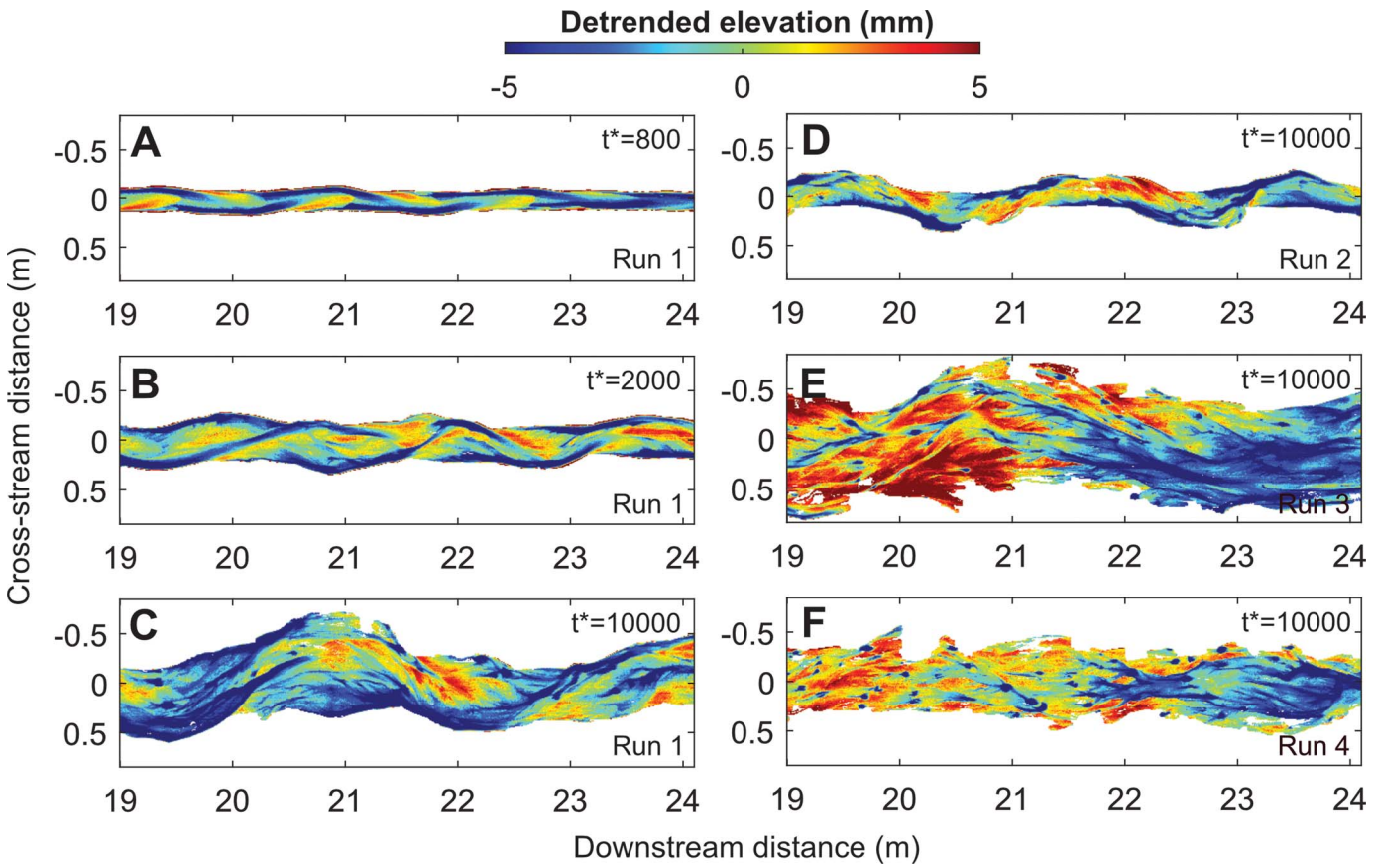

FIG. 1.—Surface evolution for all experimental runs. The first column shows the time evolution of the experimental channel in Run 1 corresponding to **A)** the meandering phase ($t^* = 800$) to **B)** the onset of braiding ($t^* = 2000$) and to **C)** channel-belt maturity ($t^* = 10{,}000$). The second column shows the detrended digital elevation models for Runs 2, 3, and 4 at the end of the braiding phase. All panels are restricted to a 5 m span alongstream. The dimensionless time (t^*; Equation 4) is shown for each panel. Details of the experimental design are explained in Limaye (2020).

erosion and deposition creates units that are bounded by pairs of successive erosional surfaces. We calculated unit thickness (s) as the thickness of the deposit between successive erosional surfaces. We filtered unit thicknesses that were smaller than 1 mm to exclude insignificant differences in elevation at the scale of the vertical precision of the measurements. We then compared the estimated unit-thickness distribution with the theoretical distribution following the Paola and Borgman (1991) model (see Equation 2). To evaluate the fit, we employed a chi-square goodness-of-fit test. We also determined the coefficient of variation of units (CV_{cf}, ratio of the standard deviation to the mean) to compare against the theoretical expectation of 0.88 (Paola and Borgman 1991). We focused our stratigraphic analysis on the second phase of the experiment ($t^* = 2000$ to 10,000), which was characterized by channel-belt widening and a braided-channel planform.

Quantifying Flow Depths Using a Two-Dimensional Flow Model

In addition to channel depths, we also quantified the changes in flow depth during each of the experimental runs (Fig. 2). Limaye (2020) did not make direct flow depth measurements due to the large scale of the basin and the difficulty of measuring *in situ* of flows that were typically less than

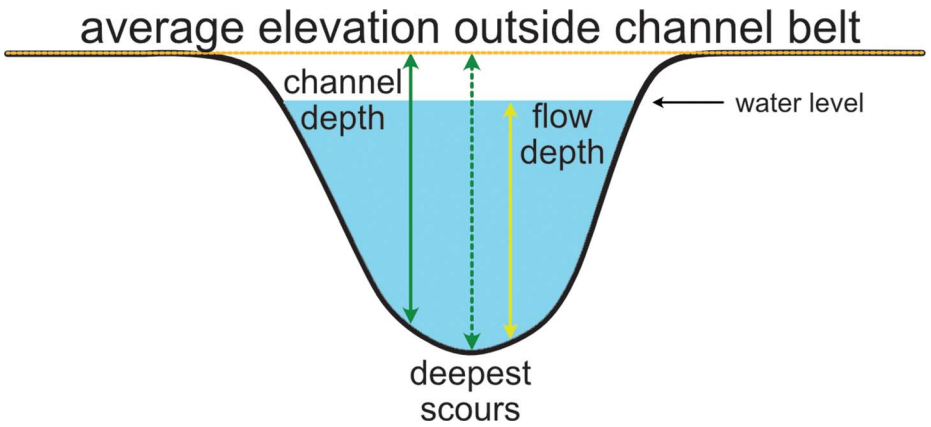

FIG. 2.—Schematic of measurements taken from elevation data. Yellow line indicates an example flow-depth measurement (h_{flow}) modeled using a reduced-complexity flow model. The solid green line indicates an example channel-depth ($h_{channel}$) measurement, which was defined as the elevation difference between the channel belt and averaged adjacent topography outside of the channel belt (dashed orange line). Channel depths greater than the 75th percentile of channel depths at each corresponding time step were classified as scour depths, while channel depths greater than the 95th percentile of channel depths referred to as the deepest scours (dashed green line).

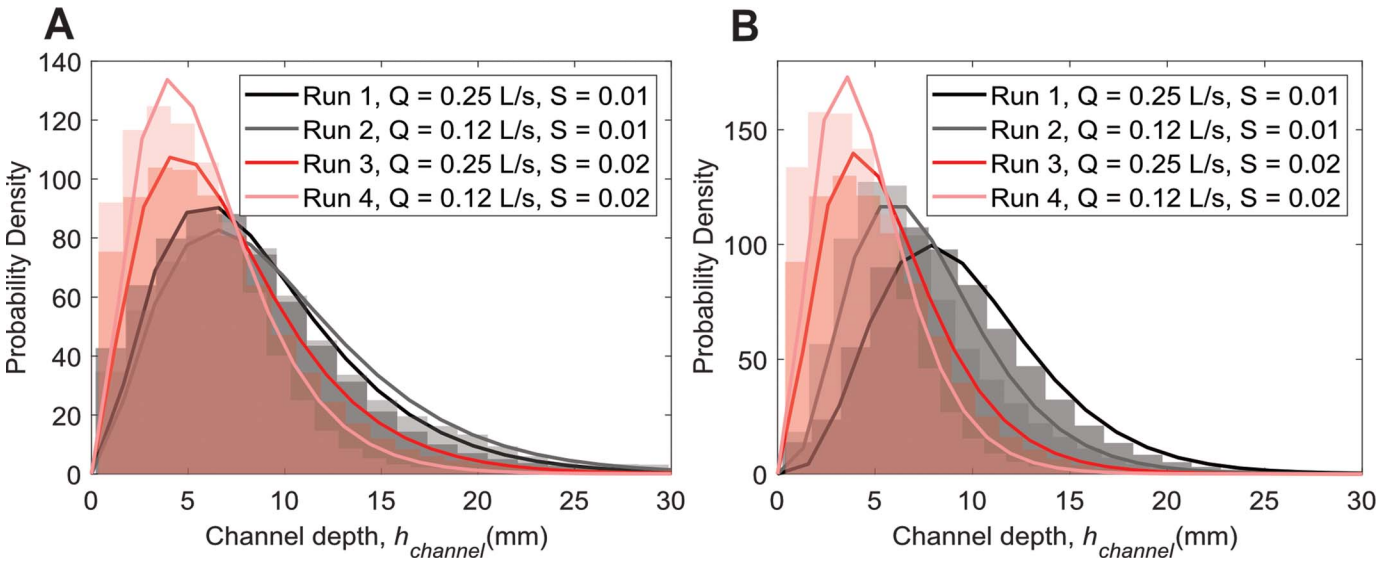

FIG. 3.—**A)** Probability density function of channel depths across all times of Run 1 ($\chi^2 = 0.07$), Run 2 ($\chi^2 = 0.04$), Run 3 ($\chi^2 = 0.04$), and Run 4 ($\chi^2 = 0.03$). **B)** Probability distribution of channel depths during the braiding phase ($t^* = 2000$ to 10000) for Run 1 ($\chi^2 = 0.3$, $\beta = 2.0$), Run 2 ($\chi^2 = 0.8$, $\beta = 1.8$), Run 3 ($\chi^2 = 0.9$, $\beta = 1.9$), and Run 4 ($\chi^2 = 1.6$, $\beta = 1.5$).

1 cm in depth. Instead, we reconstructed flow depths using a numerical model, CAESAR-lisflood (Bates et al. 2010; Coulthard et al. 2013; Limaye 2017). Using DEMs and corresponding water-discharge values as flow-model inputs, we iteratively adjusted other unmeasured flow parameters in the model until flow depths in the initial DEM of each run closely matched those observed in Limaye (2020). The model was previously similarly applied to map submarine braided channels and bars formed in physical experiments (Limaye et al. 2018) and solves a simplified version of shallow-water equations to simulate two-dimensional flow over a rectilinear grid. We calculated the width-averaged water discharge between cells as:

$$Q_{model} = \frac{q - gh_{max}\Delta t \frac{\Delta(h+z)}{\Delta t}}{1 + gh_{max}\Delta t n^2 \mid q \mid / h_{max}^{10/3}} \Delta x \quad (5)$$

where h_{max} is maximum flow depth, Δt is time step, z is bed elevation, Δx is grid spacing, and n is Manning's roughness coefficient. We propagated discharge downstream in the x and y directions until water reaches the downstream boundary and exits the domain.

To ensure accurate water routing across the DEM, we performed several preprocessing steps. First, we cropped each DEM within the range of 0 to 36.42 meters in the downstream direction and 0.1 to 2.6 meters in the cross-stream direction, effectively removing cells outside of the channel-belt mask. Second, to mimic the geometry of the laboratory basin, we introduced lateral walls along both sides of the DEM, which confined flow to the model domain until reaching the downstream outlet. Third, we downsampled each DEM by a factor of 10, resulting in a grid spacing of 2 cm, which was sufficiently large to preserve major topographic features while decreasing computation time. Finally, we fed modeled flow from an inlet point 40 mm from the upstream edge of the DEM, using a discharge equivalent to the input in each run of the experiment (Table 1). We use the model with sediment transport disabled, using the spatial pattern of inundation to map preferred routes of flow over the topography (Limaye 2017).

To tune the model to mimic hydraulic conditions in the basin, we applied a 1 mm threshold to the modeled flow depths to prevent a thin layer of flow spreading over areas of low relief (Bates et al. 2010; Coulthard et al. 2013; Limaye et al. 2018). Other model parameters included a Froude-number flow limit of 0.8 and a Courant number of 0.3. The Froude-number flow limit prevents excessive flow between cells leading to "checkerboarding" effects, and the Courant number specifies the model time step to remain within the range for numerical stability. We varied the Manning's roughness coefficient between 0.06 and 0.1, as the model was adjusted to yield initial median flow depths of 2–3 cm for an experimental run, motivated by the observation that for all runs flow nearly filled the initial channel but did not spill out to the surrounding areas (Limaye 2020). We calculated flow depths for DEMs at a fixed interval of dimensionless time ($t^* = 2000$) in each experiment during the braiding phase, i.e., when the channel-belt width grew logarithmically in time. We ran the flow model for a simulation time of 60 minutes for each DEM, which coincided with the time it took for water discharge entering and leaving the domain to equilibrate.

Similar to $h_{channel}$, we also compared the distribution of h_{flow} with a two-parameter gamma distribution (Equation 1). We also compared h_{flow} with $h_{channel}$ through time. Finally, we computed an aggregate-preservation ratio as the mean preserved unit thickness and the grand-mean formative flow depths during the braiding phase of all experimental runs. We also computed the net aggradation rate during the braiding phase of each experiment by differencing DEMs at $t^* = 10000$ and $t^* = 2000$, taking the mean value of the difference map, and dividing it by the run time. We normalized the net aggradation rate by the grand median flow depth across the braiding phase.

RESULTS

Characteristics of Channel and Flow Depth across Experiments

Runs 1 and 2 produced the largest absolute channel depths, while Runs 3 and 4 produced comparatively shallower channel depths on average (Fig. 3). During the braiding phase, the estimated median channel depth ($h_{channel}$) varied between 3.4 mm (Run 4) and 8.9 mm (Run 1), and the interquartile range (IQR) varied between 3.5 mm (Run 4) and 5.6 mm (Run 1) (Fig. 3B). Across all experiments (including the meandering, braiding, and mature channel-belt phases), the median channel depth varied between 5.5 mm (Run 4) and 8.7 mm (Run 2), and IQR varied between 4.5 mm (Run 4) and 7 mm (Run 2) (Fig. 3B). Similar to channel depths, flow depths generated by the CAESAR-lisflood flow model were greater in Runs 1 and 2 compared to Runs 3 and 4. Median flow depths varied between 3 mm (Run 4) and 9.9 mm (Run 1), and the IQR varied between 2.5 mm (Run 4) and 5.6 mm (Run 1)

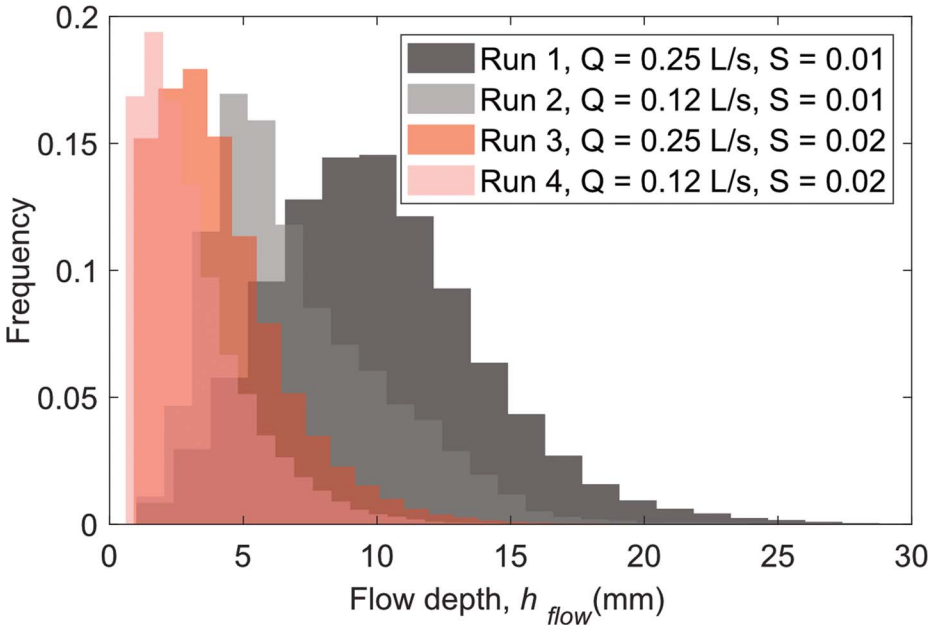

FIG. 4.—Probability density functions of modeled flow depths generated for each experimental run. Modeled flow depths were calculated for at a fixed interval of dimensionless time ($t^* = 2000$) during the braiding phase of each experimental run.

(Fig. 4). The estimated flow depths were on average 2 to 3 mm shallower than their corresponding channel depths (Fig. 5).

Both modeled flow depths and channel depths decreased as the channel belt widened, consistent with qualitative observations during the experiment (Figs. 6, 7). As such, most of the deepest scours occurred during the meandering phase of each run ($t^* = 0$ to 2000) when topographic change was highest (e.g., Bridge 2003; Holbrook and Allen 2020). We identified the locations of scours (> 75th percentile of channel depths) during the braiding phase ($t^* = 2000$ to 10,000) and found that scours persistently occurred near the channel margins as bend-apex pools, and at channel-thread confluences during the braiding phase of all experiment runs (Figs. 6, 7). Across all runs, the deepest scours (> 95th percentile of the channel depths) were 2.0 (Run 1) to 4.3 times (Run 4) greater than the mean flow depth computed across the entire braiding phase of experiment runs.

We found that the two-parameter gamma distribution adequately described the channel-depth distributions for each run for all time steps and time steps restricted to the braiding phase ($t^* = 2000$ to 10,000) (Fig. 6A, B). The χ^2 values for the fitted density function were below the critical value at the $\alpha = 0.05$ significance level. The scale parameter of the channel-depth distribution, which is hypothesized to control the distribution of preserved unit thickness (Paola and Borgman 1991), varied from 1.5 to 2.0 across the braiding phase of Runs 1 and 4, respectively.

Characteristics of Preserved Cut-and-Fill Unit Thickness across Experiments

Figure 8 shows example cross sections of the preserved stratigraphy across all four experimental runs. Our results show that the unit thickness distributions across the four runs were similar to each other. The estimated median unit thickness varied between 2.3 mm (Run 2) and 2.7 mm (Run 3), and the IQR varied between 2 mm (Run 2) and 2.8 mm (Run 3). The thickest units ranged from 10 to 31 mm in all runs and were deposited mainly through

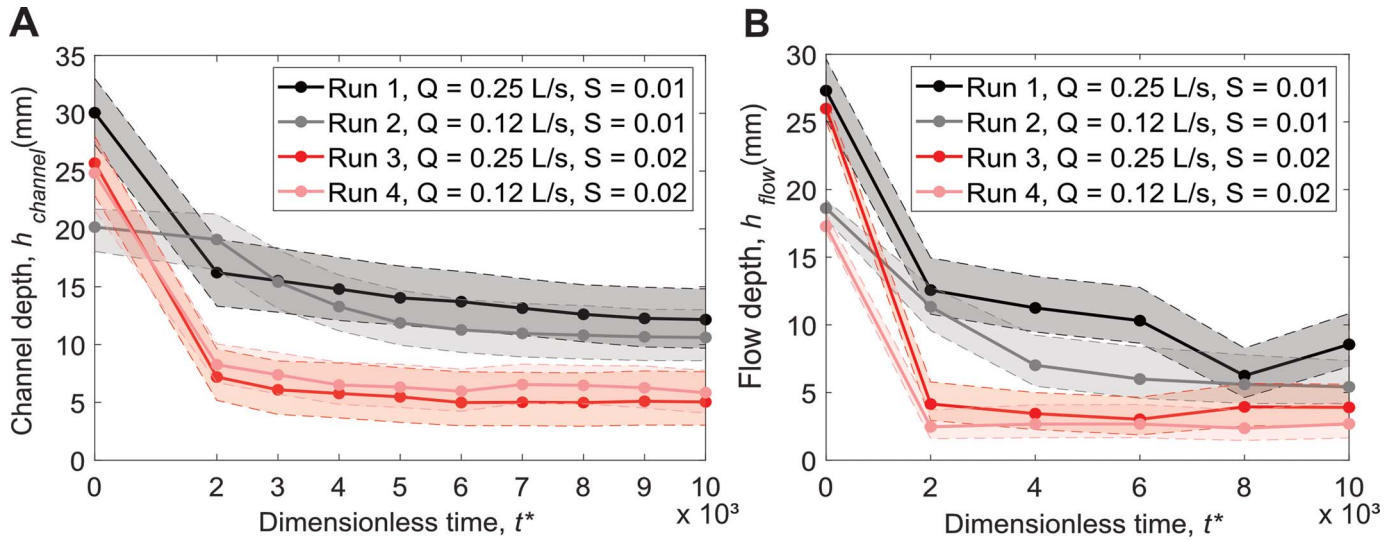

FIG. 5.—Time series of median **A)** channel depths ($h_{channel}$) and **B)** modeled flow depths (h_{flow}) for the braiding phase ($t^* = 2000$ to 10,000) and at $t^* = 0$. Dashed lines indicate the 25th and 75th percentiles of each parameter.

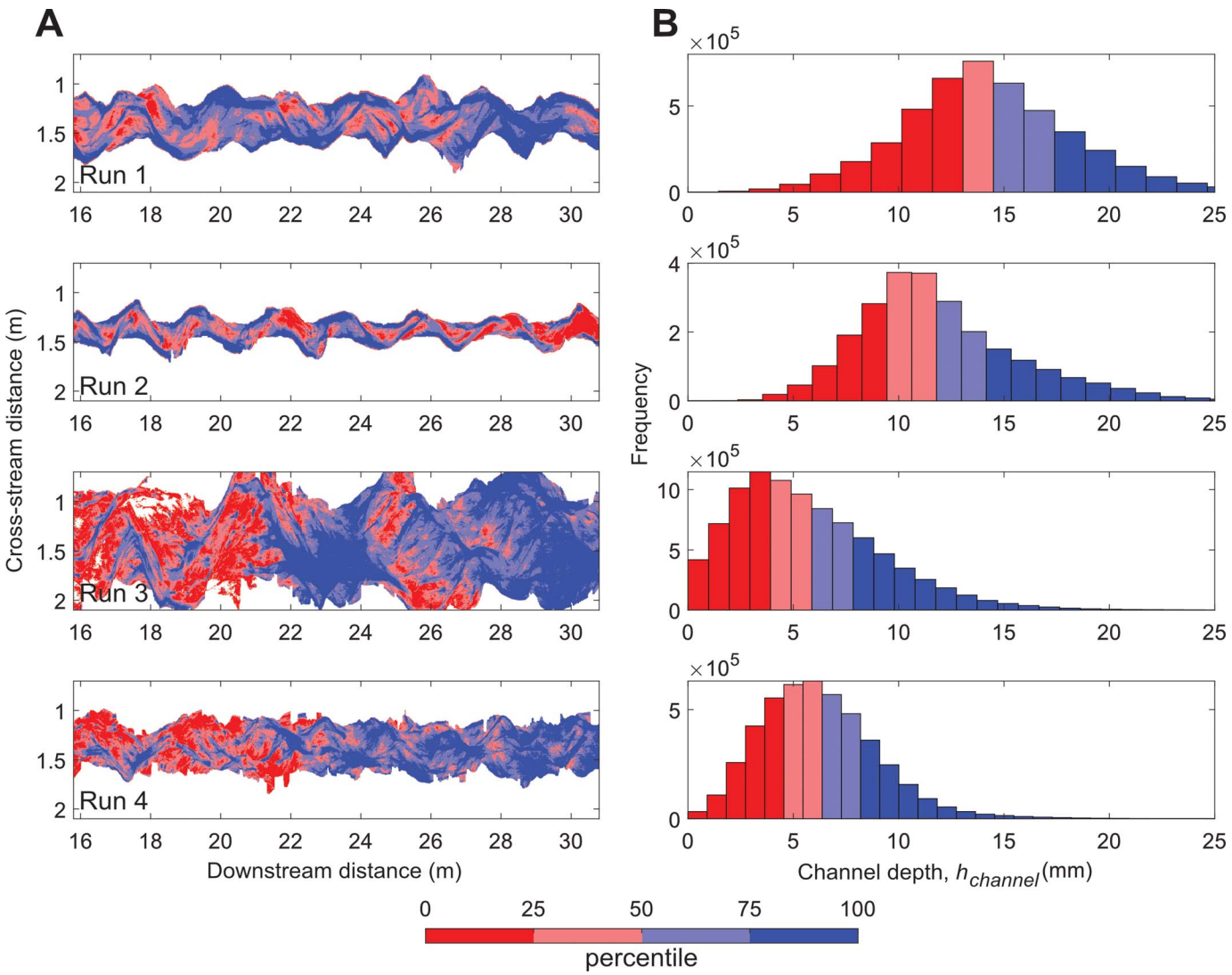

FIG. 6.—Channel depths color-coded based on percentile for each run. All panels are restricted to a 15 m extent at $t^* = 6000$. **A)** Map view of channel depths where lighter blue represents scours and dark blue represents the deepest scours. **B)** Corresponding histograms. The largest scours (> 95th percentile) occur at the channel-belt margins and confluence scours in the channel belt.

overall aggradation of the channel bed over time as material was eroded from the margins of the channel belt and deposited on the bed. This aggradation trend has been previously observed for a similar experimental setup (Hirano 1973; Limaye 2020).

Overall, all the unit-thickness distributions were well described by the theoretical distribution proposed by Paola and Borgman (1991), shown in Equation 2. The coefficient of variation of the preserved unit thickness ranged between 0.67 (Run 4) and 0.73 (Run 1) and is in close agreement with the theoretical value of 0.88 (Paola and Borgman 1991), and within the empirical range of 0.58 to 1.18 proposed by Bridge and Best (1997) for variability-dominated preservation in fluvial strata. The χ^2 values for the fitted density function were below the critical value at the $\alpha = 0.05$ significance level, which indicates the predicted density function is an adequate fit of the data (Fig. 9).

Our results also revealed that the preserved-unit-thickness distribution can be predicted from the channel-depth distribution, and vice versa, in all experimental runs. The predicted mean unit thickness using the scale parameter of fitted gamma distributions for the channel depths were 3.3 mm, 3.0 mm, 3.1 mm, and 2.5 mm for Runs 1, 2, 3, and 4, respectively. These values agree with the observed mean unit thickness of 3.1 mm, 3.1 mm, 2.9 mm, and 2.8 mm for Runs 1, 2, 3, and 4, respectively (Fig. 10A). We found that the aggregate preservation ratio, calculated as the mean unit thickness divided by the mean flow depth, was 0.38, 0.31, 0.49, and 0.62 for Runs 1 through 4, respectively (Fig. 10B). The differences in aggregate preservation ratios reflect the differences in the formative flow depths as unit thickness remains consistent between experimental runs. Moreover, we found that the differences in aggregate preservation ratio correlated with the estimated net aggradation rates observed from the experiments. We found that the mean net aggradation rate was 0.21 mm/hour, 0.29 mm/hour, 0.18 mm/hour, and 0.15 mm/hour for Runs 1, 2, 3, and 4, respectively. The normalized net aggradation rates were 0.02 $hour^{-1}$, 0.04 $hour^{-1}$, 0.05 $hour^{-1}$, and 0.05 $hour^{-1}$ for the braiding phase of Runs 1 through 4, respectively. Therefore, our results indicate that the highest aggregate preservation ratios occurred in experiments with largest net normalized aggradation rates.

DISCUSSION

We analyzed data from an experiment in which braided rivers exhibited channel belts that evolved under conditions of constant sediment and

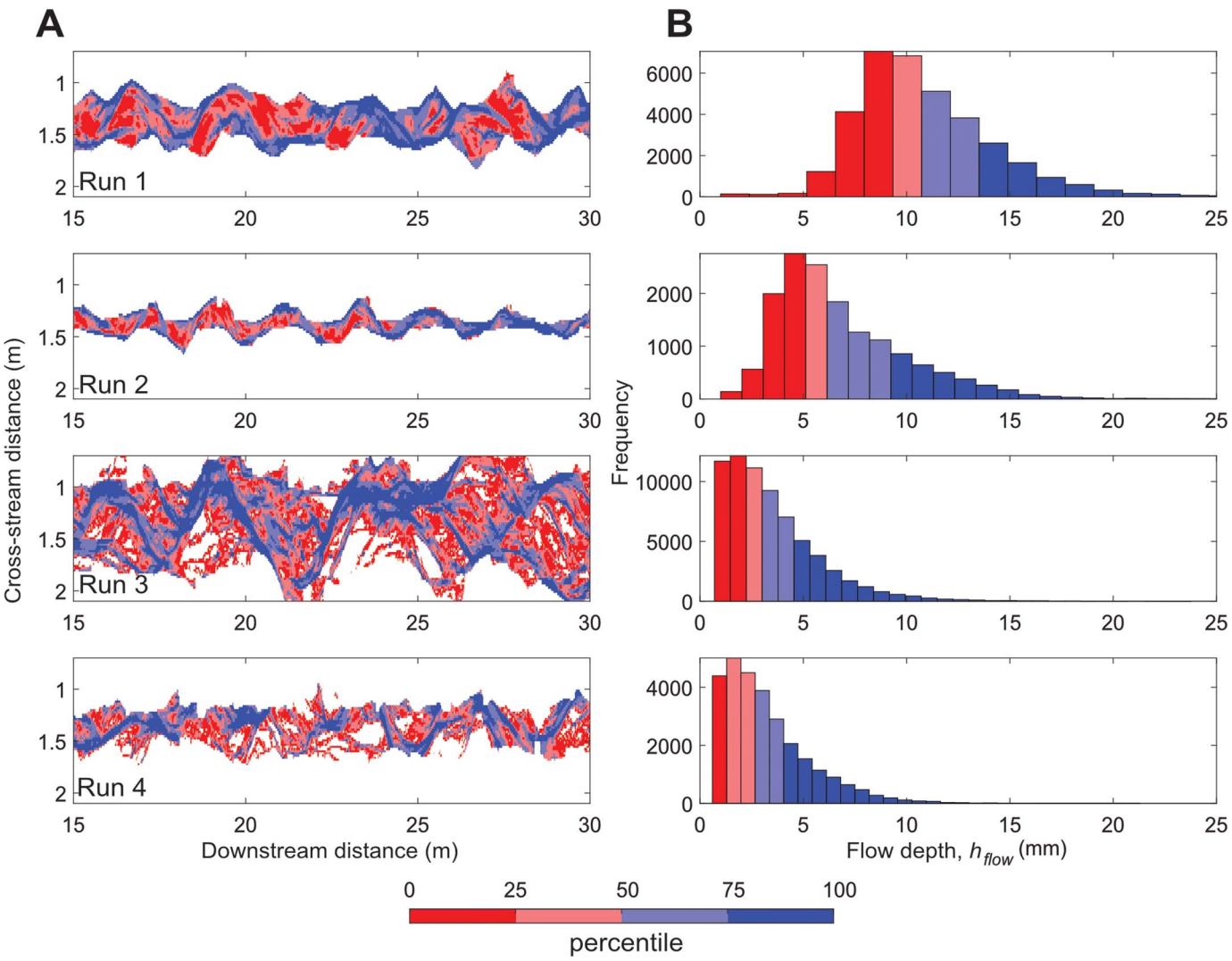

FIG. 7.—Modeled flow depth (h_{flow}), color-coded by percentile for the four experimental runs. All panels are restricted to a 15 m extent and shown at the same dimensionless time ($t^* = 6000$). **A)** Map views of flow depths, where dark blue represents the largest flow depths. **B)** Histograms of the estimated flow depths.

water discharge. We mapped channels and flow depths using a reduced-complexity flow model, quantified the spatiotemporal evolution of channel depths, and constructed synthetic stratigraphy from bed-elevation evolution to compare our results with a variability-dominated preservation model of Paola and Borgman (1991).

Our key finding is that the synthetic stratigraphy constructed across all four runs were indistinguishable (Fig. 10A). In other words, a two-fold change in water discharge and slope in the experiment did not lead to an identifiable change in the preserved unit thickness. This result supports other experimental studies (van de Lageweg et al. 2013b) where synthetic stratigraphy did not vary noticeably despite varying water discharge in experiment runs. Our results indicate that to cause a change in preserved-unit-thickness distribution, the variation in external conditions need to cause a significant change in the extreme channel depths (i.e., scours) because the preserved unit thickness is a function of the scour-depth variability. These results support the notion that large rivers may buffer signals resulting from variations in sediment flux, water discharge, or slope because changes in external conditions are unlikely to cause sufficiently large changes that surmount the autogenic variability in channel depths of large fluvial systems (Ganti et al. 2014; Hajek and Straub 2017). These findings also suggest an important outstanding question: How large a change in external forcing is required to cause an identifiable change in the preserved cut-and-fill-unit geometry of braided-river deposits?

Further, in natural rivers, variations in water discharge and slope can also be compensated by parameters other than channel depth, such as channel-belt width and braiding index (Holbrook and Allen 2020), which are not expressed directly in unit thickness. Limaye (2020) demonstrated that runs with higher discharge and slope (Run 3) grew wider channel belts than runs with lower discharge and slope (Run 2), suggesting that the lack of an identifiable change in preserved unit thickness may be attributed to major changes in channel-belt width as opposed to channel depth. Given the fourfold variation in stream power between Run 3 and Run 2, the channel-belt width in Run 3 was four times greater than in Run 2 at the end of the braiding phase, while the mean channel depth for Run 3 differed only by a factor of 1.3 compared to Run 2. These observations indicate that the signal of external changes in water discharge and stream power are likely buffered in channel-depth variations and preserved unit thickness, and channel-belt widths may be a better indicator of external variations in water discharge of braided rivers. We suggest that these predictions should be further tested in future experiments where riverbed slope dynamically adjusts to sediment feed rate (e.g., Ashworth et al.

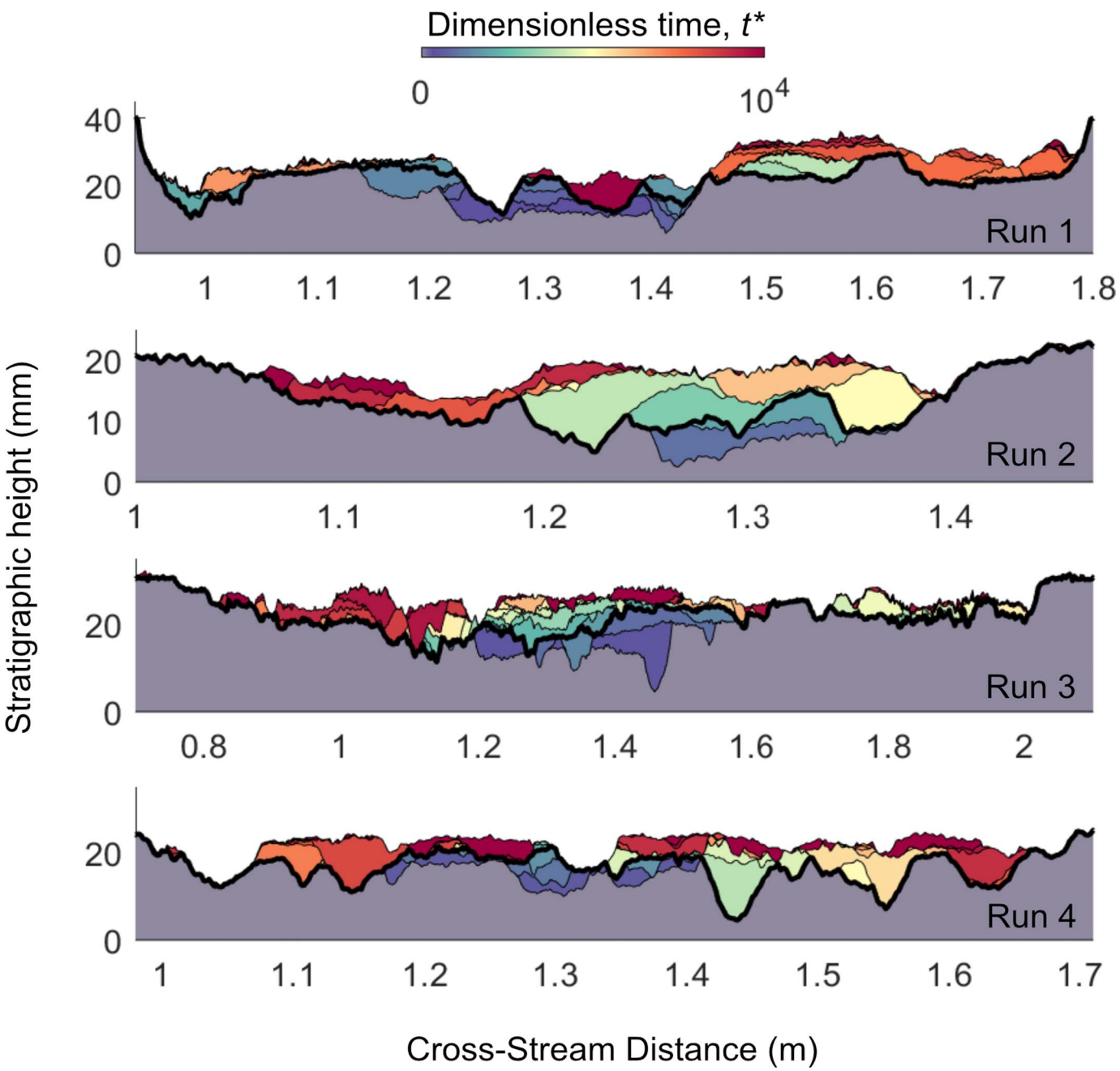

FIG. 8.—Synthetic stratigraphic section generated from stacked DEMs, clipped for erosion. The cross sections were taken every 2 mm downstream. Deposits are colored by dimensionless time of deposition. Black lines denote the erosional surfaces and represent contours of constant dimensionless time. The dark black line corresponds to the onset of the braiding phase ($t^* = 2000$ to 10,000).

2004, 2007), which contrasts our experimental setup where low sediment supply and long equilibrium timescales effectively rendered slope as an independent parameter between experiments.

Estimates of paleoflow depths from outcrop successions are important for reconstructing channel slopes, water discharges, and sediment fluxes of ancient river systems. For example, proxy estimates of flow depths can be directly obtained from unit-thickness measurements of fully preserved bar-scale strata (Bridge and Tye 2000; Mohrig et al. 2000; Alexander et al. 2020), which set the upper bound of flow depths. Here, we found that the aggregate preservation ratio varied between 0.31 (Run 2) and 0.62 (Run 4), implying that the preserved unit thickness represents 31% to 62% of the original channel depth across all experimental runs. The observed variations in aggregate preservation ratios across runs can be attributed to different net aggradation rates. As such, lower aggradation rates lead to smaller preservation ratios. For example, Paola and Borgman (1991) reported predicted preservation ratios between 0.4 and 0.75 for modern braided river channels, which compare well with data from Runs 3 and 4. On the other hand, van de Lageweg et al. (2013b) reported lower preservation ratios between 0.1 and 0.4 for experimental gravel-bed rivers in the absence of aggradation; these values compare well with aggregate preservation ratios from Runs 1 and 2. Future work could address how preservation ratio also varies with river system scale, especially in the context of larger rivers that are characterized by deeper

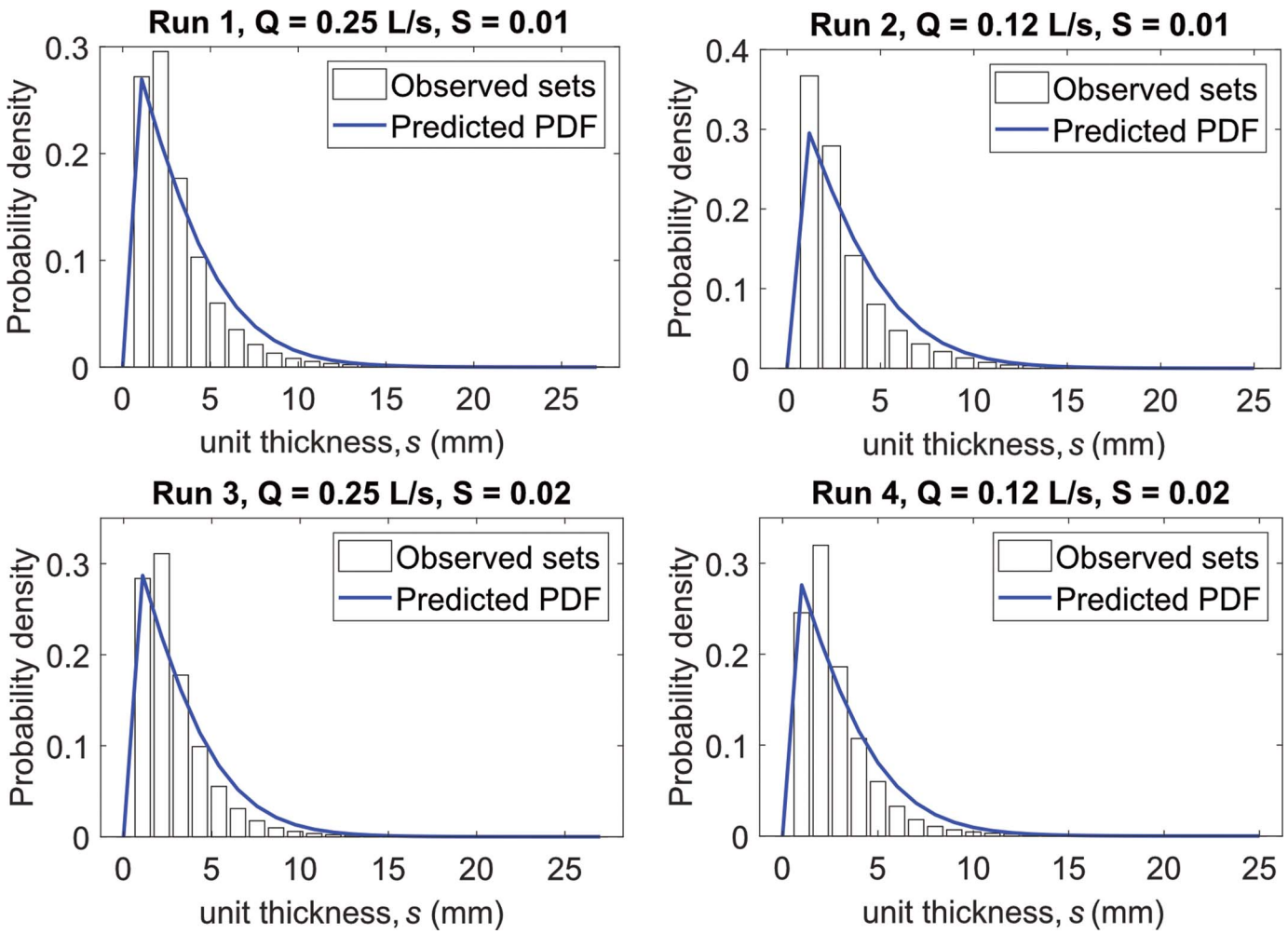

FIG. 9.—Preserved cut-and-fill-unit thickness measured across the four experimental runs, plotted alongside the theoretical probability density function (Equation 2). The chi-square test indicates that Equation 2 adequately fits unit thickness distributions for Run 1 ($\chi^2 = 0.04$, $CV_{cf} = 0.73$), Run 2 ($\chi^2 = 0.08$, $CV_{cf} = 0.73$), Run 3 ($\chi^2 = 0.04$, $CV_{cf} = 0.69$), and Run 4 ($\chi^2 = 0.03$, $CV_{cf} = 0.67$).

channels, varied channel spacing, and faster channel migration (Castelltort 2018; Li et al. 2023).

Our results also add further evidence that a reduced-complexity flow model can be combined with topography measurements to generate more data from existing experiments where *in situ* flow measurements are challenging (e.g., Baynes et al. 2018; Limaye et al. 2018). We used a two-dimensional flow model to generate maps of flow-depth evolution and found that the estimated flow depths and channel depths were similar to each other in the experimental runs because channels were at or near bankfull conditions (Figs. 3, 4; Limaye 2020). The deepest scours in braided-channel belts occur along the channel-belt margins as bend-apex pools and near the confluences of individual channel threads (Fig. 6). In addition, we found that the deepest scour depths in the experimental braided rivers were 2.0 (Run 1) to 4.3 times (Run 4) greater than the mean modeled flow depth. This finding aligns with natural braided rivers where maximum channel depths were observed to be as much as three to five times the mean flow depth (Best and Ashworth 1997). Both flow depth and channel depths were greater for Runs 1 and 2 than for Runs 3 and 4, which we attribute to the difference in slopes. Runs 3 and 4 had a larger bed slope by a factor of two and aggraded much faster than Runs 1 and 2 (Fig. 5A, B), thus producing shallower flow depths and channel depths.

Finally, our results agree with the variability-dominated preservation model proposed by Paola and Borgman (1991) and indicates that the tail parameter of flow-depth and channel-depth distributions is more important in setting the unit-thickness distribution of braided river deposits than median values. Although the Paola and Borgman (1991) theory assumes no net deposition, we find that their variability-dominated preservation model is valid for braided channels even in the presence of aggradation. This observation is consistent with numerical and experimental models of bedform preservation where deviations from the variability-dominated preservation model have been shown to occur only at high ratios of bedform aggradation rate to migration rate (Bridge and Best 1997; Leclair 2002; Jerolmack and Mohrig 2005). Together these results suggest that the variability-dominated preservation model could be widely applicable for reconstructing formative flow depths from braided-river deposits.

CONCLUSIONS

We mapped channel depths and preserved unit thickness for four experimental runs of a braided river with varying bed slope and water discharge. We evaluated Paola and Borgman (1991) theory for reconstructing surface morphology from the preserved stratigraphy and estimated flow depths using a two-dimensional flow model, CAESAR-lisflood. This analysis shows that:

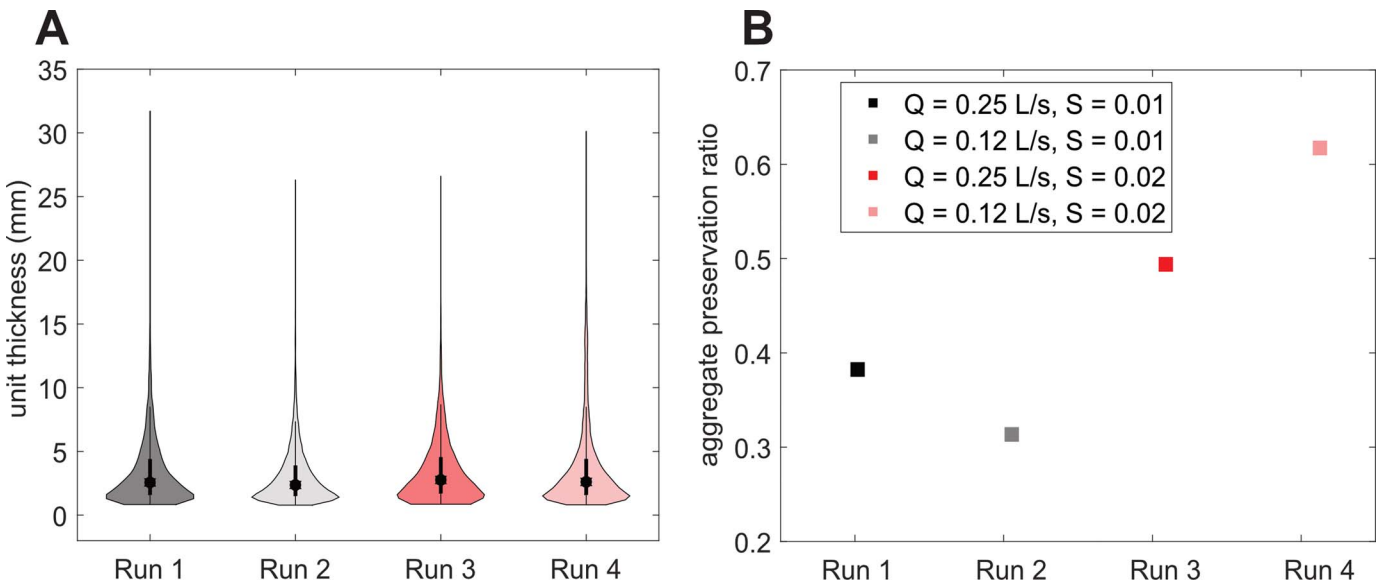

FIG. 10.—**A)** Comparison of preserved cut-and-fill-unit thickness across the four experiment runs. **B)** Aggregate preservation ratio for all runs, calculated as the mean cut-and-fill-unit thickness divided by the mean flow depth.

1. Measured channel depths are well described by a two-parameter gamma distribution. Spatially, maximum channel depths correspond with erosion at channel-belt margins and confluence scours in the channel belt. The deepest scours were 2.0 to 4.3 times larger than mean flow depths, consistent with field observations from modern braided rivers.
2. Cut-and-fill unit-thickness distributions in the laboratory experiment were consistent with the variability-dominated preservation model of Paola and Borgman (1991), which suggests that the theory is valid for braided rivers and their deposits at the channel scale. Further, the aggregate preservation ratio varied between 0.31 to 0.62 and correlated with net aggradation rates in the experiment, indicating that measured unit thickness can be used to reconstruct flow depths.
3. A two-fold change in water discharge and/or initial bed slope is not recorded in the preserved unit thickness but is reflected in the channel-belt width. This observation suggests that changes in median channel depth will not manifest as changes in unit thickness until a certain threshold in water discharge and slope is reached—a threshold not reached in our experiments.
4. Flow depths calculated using the CAESAR-lisflood model were 2 to 3 mm shallower than corresponding channel depths, indicating that the model was effective in accurately routing water across the DEMs.

ACKNOWLEDGMENTS

This work was supported by the National Science Foundation grant EAR 1935669 to Ganti. Physical experiments analyzed in this work were supported by the donors to the American Chemical Society.

REFERENCES

ALEXANDER, J.S., MCELROY, B.J., HUZURBAZAR, S., AND MURR, M.L., 2020, Elevation gaps in fluvial sandbar deposition and their implications for paleodepth estimation: Geology, v. 48, p. 718–722.

ALLEN, J.R.L., 1984, Sedimentary Structures, Their Character and Physical Basis: Amsterdam, Elsevier Scientific Publishing Company, 593 p.

ANDERSON, M.P., AIKEN, J.S., WEBB, E.K., AND MICKELSON, D.M., 1999, Sedimentology and hydrogeology of two braided stream deposits: Sedimentary Geology, v. 129, p. 187–199.

ASHMORE, P.E., 1991, How do gravel-bed rivers braid?: Canadian Journal of Earth Sciences, v. 28, p. 326–341.

ASHMORE, P., 1993, Anabranch confluence kinetics and sedimentation processes in gravel-braided streams, *in* Best, J.L., and Bristow C.S., eds., Braided Rivers: Geological Society of London, Special Publication 75, p. 129–146.

ASHMORE, P., 2013, Morphology and dynamics of braided rivers, *in* Shroder, J.F., ed., Treatise on Geomorphology: San Diego, Academic Press, p. 289–312.

ASHMORE, P., AND GARDNER, J.T., 2008, unconfined confluences in braided rivers, *in* Rice, S., Roy, A., and Rhoads, B., eds., River Confluences, Tributaries and the Fluvial Network: John Wiley and Sons, p. 119–147.

ASHMORE, P., AND PARKER, G., 1983, Confluence scour in coarse braided streams: Water Resources Research, v. 19, p. 392–402.

ASHWORTH, P.J., BEST, J.L., AND JONES, M., 2004, Relationship between sediment supply and avulsion frequency in braided rivers: Geology, v. 32, p. 21–24.

ASHWORTH, P.J., BEST, J.L., AND JONES, M., 2007, The relationship between channel avulsion, flow occupancy and aggradation in braided rivers: insights from an experimental model: Sedimentology, v. 54, p. 497–513.

BATES, P.D., HORRITT, M.S., AND FEWTRELL, T.J., 2010, A simple inertial formulation of the shallow water equations for efficient two-dimensional flood inundation modelling: Journal of Hydrology, v. 387, p. 33–45.

BAYNES, E.R.C., LAGUE, D., AND KERMARREC, J.-J., 2018, Supercritical river terraces generated by hydraulic and geomorphic interactions: Geology, v. 46, p. 499–502.

BEST, J.L., AND ASHWORTH, P.J., 1997, Scour in large braided rivers and the recognition of sequence stratigraphic boundaries: Nature, v. 387, p. 275–277.

BRIDGE, J.S., 2003, Rivers and Floodplains: Forms, Processes, and Sedimentary Record: Oxford, Blackwell, 491 p.

BRIDGE, J.S., AND BEST, J., 1997, Preservation of planar laminae due to migration of low-relief bed waves over aggrading upper-stage plane beds: comparison of experimental data with theory: Sedimentology, v. 44, p. 253–262.

BRIDGE, J.S., AND TYE, R.S., 2000, Interpreting the dimensions of ancient fluvial channel bars, channels, and channel belts from wireline-logs and cores: American Association of Petroleum Geologists, Bulletin, v. 84, p. 1205–1228.

CASTELLTORT, S., 2018, Empirical relationship between river slope and the elongation of bars in braided rivers: a potential tool for paleoslope analysis from subsurface data: Marine and Petroleum Geology, v. 96, p. 544–550.

COULTHARD, T.J., NEAL, J.C., BATES, P.D., RAMIREZ, J., DE ALMEIDA, G.A.M., AND HANCOCK, G.R., 2013, Integrating the LISFLOOD-FP 2D hydrodynamic model with the CAESAR model: implications for modelling landscape evolution: Earth Surface Processes and Landforms, v. 38, p. 1897–1906.

DADE, W.B., AND FRIEND, P.F., 1998, Grain-size, sediment-transport regime, and channel slope in alluvial rivers: The Journal of Geology, v. 106, p. 661–676.

DAS, D., GANTI, V., BRADLEY, R., VENDITTI, J., REESINK, A., AND PARSONS, D.R., 2022, The influence of transport stage on preserved fluvial cross strata: Geophysical Research Letters, v. 49, e2022GL099808.

DUNNE, K.B., AND JEROLMACK, D.J., 2020, What sets river width?: Science Advances, v. 6, p. 1–9.

FRIEDKIN, J.F., 1945, A Laboratory Study of the Meandering of Alluvial Rivers: Waterways Experimental Station: Vicksburg, Mississippi, US Army Corps of Engineers, 40 p.

GANTI, V., STRAUB, K.M., FOUFOULA-GEORGIOU, E., AND PAOLA, C., 2011, Space-time dynamics of depositional systems: experimental evidence and theoretical modeling of heavy-tailed statistic: Journal of Geophysical Research, Earth Surface, v. 116, F02011.

Ganti, V., Paola, C., and Foufoula-Georgiou, E., 2013, Kinematic controls on the geometry of the preserved cross sets: Journal of Geophysical Research: Earth Surface, v. 118, p. 1296–1307.

Ganti, V., Lamb, M.P., and McElroy, B., 2014, Quantitative bounds on morphodynamics and implications for reading the sedimentary record: Nature Communications, v. 5, p. 1–7.

Ganti, V., Whittaker, A.C., Lamb, M.P., and Fischer, W.W., 2019, Low-gradient, single-threaded rivers prior to greening of the continents: National Academy of Sciences [USA], Proceedings, v. 116, p. 11,652–11,657.

Gardner, J.T., and Ashmore, P.E., 2011, Geometry and grain-size characteristics of the basal surface of a braided river deposit: Geology, v. 39, p. 247–250.

Hajek, E.A., and Edmonds, D.A., 2014, Is river avulsion style controlled by floodplain morphodynamics?: Geology, v. 42, p. 199–202.

Hajek, E.A., and Straub, K.M., 2017, Autogenic sedimentation in clastic stratigraphy: Annual Review of Earth and Planetary Sciences, v. 45, p. 681–709.

Hirano, M., 1973, River-bed variation with bank erosion: Japan Society of Civil Engineers, Proceedings, v. 210, p. 13–20.

Holbrook, J., 2001, Origin, genetic interrelationships, and stratigraphy over the continuum of fluvial channel-form bounding surfaces: an illustration from middle Cretaceous strata, southeastern Colorado: Sedimentary Geology, v. 144, p. 179–222.

Holbrook, J.M., and Allen, S.D., 2021, The case of the braided river that meandered: bar assemblages as a mechanism for meandering along the pervasively braided Missouri River, USA: Geological Society of America, Bulletin, v. 133, p. 1505–1530.

Holbrook, J.M., and Miall, A.D., 2020, Time in the rock: a field guide to interpreting past events and processes from siliciclastic stratigraphy: Earth-Science Reviews, v. 203, no. 103121, 23 p.

Holbrook, J., and Wanas, H., 2014, A fulcrum approach to assessing source-to-sink mass balance using channel paleohydrologic parameters derivable from common fluvial data sets with an example from the Cretaceous of Egypt: Journal of Sedimentary Research, v. 84, p. 349–372.

Huber, E., and Huggenberger, P., 2015, Morphological perspective on the sedimentary characteristics of a coarse, braided reach: Tagliamento River (NE Italy): Geomorphology, v. 248, p. 111–124.

Jerolmack, D.J., and Mohrig, D., 2005, Frozen dynamics of migrating bedforms: Geology, v. 33, p. 57–60.

Leclair, S.F., 2002, Preservation of cross-strata due to the migration of subaqueous dunes: an experimental investigation: Sedimentology, v. 49, p. 1157–1180.

Li, W., Colombera, L., Yue, D., and Mountney, N.P., 2023, Controls on the morphology of braided rivers and braid bars: an empirical characterization of numerical models: Sedimentology, v. 70, p. 259–279.

Limaye, A.B., 2017, Extraction of multithread channel networks with a reduced-complexity flow model: Journal of Geophysical Research, Earth Surface, v. 122, p. 1972–1990.

Limaye, A.B., 2020, How do braided rivers grow channel belts?: Journal of Geophysical Research, Earth Surface, v. 125, e2020JF005570.

Limaye, A.B., Grimaud, J.-L., Lai, S.Y.J., Foreman, B.Z., Komatsu, Y., and Paola, C., 2018, Geometry and dynamics of braided channels and bars under experimental density currents: Sedimentology, v. 65, p. 1947–1972.

Marren, P.M., 2005, Magnitude and frequency in proglacial rivers: a geomorphological and sedimentological perspective: Earth-Science Reviews, v. 70, p. 203–251.

Martin, J.H., 1993, A review of braided fluvial hydrocarbon reservoirs: the petroleum engineer's perspective, *in* Best, J.L., and Bristow, C.S., eds., Braided Rivers: Geological Society of London, Special Publication 75, p. 333–367.

Miall, A.D., 1985, Architectural-element analysis: a new method of facies analysis applied to fluvial deposits: Earth-Science Reviews, v. 22, p. 261–308.

Miall, A.D., and Jones, B.G., 2003, Fluvial architecture of the Hawkesbury Sandstone (Triassic), near Sydney, Australia: Journal of Sedimentary Research, v. 73, p. 531–545.

Mohrig, D., Heller, P.L., Paola, C., and Lyons, W.J., 2000, Interpreting avulsion process from ancient alluvial sequences: Guadalope–Matarranya system (northern Spain) and Wasatch Formation (western Colorado): Geological Society of America, Bulletin, v. 112, p. 1787–1803.

Paola, C., 2000, Quantitative models of sedimentary basin filling: Sedimentology, v. 47, p. 121–178.

Paola, C., and Borgman, L., 1991, Reconstructing random topography from preserved stratification: Sedimentology, v. 38, p. 553–565.

Paola, C., and Mohrig, D., 1996, Palaeohydraulics revisited: palaeoslope estimation in coarse-grained braided rivers: Basin Research, v. 8, p. 243–254.

Paola, C., Straub, K., Mohrig, D., and Reinhardt, L., 2009, The unreasonable effectiveness of stratigraphic and geomorphic experiments: Earth-Science Reviews, v. 97, p. 1–43.

Parker, G., 1978, Self-formed straight rivers with equilibrium banks and mobile bed: part 1, the sand–silt river: Journal of Fluid Mechanics, v. 89, p. 109–125.

Peakall, J., Ashworth, P.J., and Best, J.L., 2007, Meander-bend evolution, alluvial architecture, and the role of cohesion in sinuous river channels: a flume study: Journal of Sedimentary Research, v. 77, p. 197–212.

Reesink, A.J.H., van den Berg, J.H., Parsons, D.R., Amsler, M.L., Best, J.L., Hardy, R.J., Orfeo, O., and Szupiany, R.N., 2015, Extremes in dune preservation: controls on the completeness of fluvial deposits: Earth-Science Reviews, v. 150, p. 652–665.

Sambrook Smith, G.H., Ashworth, P.J., Best, J.L., Woodward, J., and Simpson, C.J., 2005, The morphology and facies of sandy braided rivers: some considerations of scale invariance, *in* Blum, M.D., Marriott, S.B., and Leclair, S.F., eds., Fluvial Sedimentology VII: Oxford, Blackwell Publishing, p. 145–158.

Sambrook Smith, G.H., Ashworth, P.J., Best, J.L., Woodward, J., and Simpson, C.J., 2006, The sedimentology and alluvial architecture of the sandy braided South Saskatchewan River, Canada: Sedimentology, v. 53, p. 413–434.

Sambrook Smith, G.H., Nicholas, A.P., Best, J.L., Bull, J.M., Dixon, S.J., Goodbred, S., Sarker, M.H., and Vardy, M.E., 2019, The sedimentology of river confluences: Sedimentology, v. 66, p. 391–407.

Schlager, W., 1993, Accommodation and supply: a dual control on stratigraphic sequences: Sedimentary Geology, v. 86, p. 111–136.

Straub, K.M., and Esposito, C.R., 2013, Influence of water and sediment supply on the stratigraphic record of alluvial fans and deltas: process controls on stratigraphic completeness: Journal of Geophysical Research, Earth Surface, v. 118, p. 625–637.

Straub, K.M., Ganti, V., Paola, C., and Foufoula-Georgiou, E., 2012, Prevalence of exponential bed thickness distributions in the stratigraphic record: experiments and theory: Journal of Geophysical Research, Earth Surface, v. 117, F02003.

Strong, N., and Paola, C., 2008, Valleys that never were: time surfaces versus stratigraphic surfaces: Journal of Sedimentary Research, v. 78, p. 579–593.

Trower, E.J., Ganti, V., Fischer, W.W., and Lamb, M.P., 2018, Erosional surfaces in the Upper Cretaceous Castlegate Sandstone (Utah, USA): sequence boundaries or autogenic scour from backwater hydrodynamics?: Geology, v. 46, p. 707–710.

van de Lageweg, W.I., van Dijk, W.M., and Kleinhans, M.G., 2013a, Channel belt architecture formed by a meandering river: Sedimentology, v. 60, p. 840–859.

van de Lageweg, W.I., Van Dijk, W.M., and Kleinhans, M.G., 2013b, Morphological and stratigraphical signature of floods in a braided gravel-bed river revealed from flume experiments: Journal of Sedimentary Research, v. 83, p. 1033–1046.

van Dijk, W.M., van de Lageweg, W.I., and Kleinhans, M.G., 2013, Formation of a cohesive floodplain in a dynamic experimental meandering river: Earth Surface Processes and Landforms, v. 38, p. 1550–1565.

Willis, B.J., and Behrensmeyer, A.K., 1994, Architecture of Miocene overbank deposits in northern Pakistan: Journal of Sedimentary Research, v. 64, p. 60–67.

Received 16 November 2023; accepted 20 April 2020.